Fall 11-15-2019

Measurement of Photoionization Rates in Air

Justin K. Smith

Justin K. Smith

Candidate

Electrical and Computer Engineering

Department

This thesis is approved, and it is acceptable in quality and form for publication:

Approved by the Thesis Committee:

Dr. Jane Lehr, Chairperson

Dr. Mark Gilmore

Dr. Andrew Fierro

MEASUREMENT OF PHOTOIONZATION RATES IN AIR

by

JUSTIN K. SMITH

B.S, ELECTRICAL ENGINEERING, UNIVERSITY OF NEW MEXICO, 2017

THESIS

Submitted in Partial Fulfillment of the
Requirements for the Degree of

MASTER OF SCIENCE
ELECTRICAL ENGINEERING

The University of New Mexico
Albuquerque, New Mexico

DECEMBER, 2019

ACKNOWLEDGEMENTS

I would like to thank my advisor and thesis committee chair Dr. Jane Lehr for her invaluable guidance and support throughout this entire process. I am grateful for opportunity she has given me.

I would also like to thank the committee members, Dr. Mark Gilmore and Dr. Andrew Fierro for their time reviewing my thesis and being on my committee.

I would to acknowledge Dr. Lisa Fisher and Jon Cameron Pouncey for their help and support. They were always willing to answer questions, guide me in the right direction and provide valuable advice.

I would like to thank Cameron Harjes for our many discussions about our projects.

I would like to acknowledge our undergraduate students Isaac Garcia and Nikita Dougan for their help in fabricating materials and aiding in the data collection process. Their help has been invaluable throughout this process.

Finally, I would like to thank Alma Sanchez for her support, encouragement and patience in helping me achieve my goals. I am grateful for all that you have done. Thank you for always being there for me.

This work was supported in part by the U.S. Office of Naval Research under Contract STTR N00014-16-C-1038.

MEASUREMENTS OF PHOTOIONIZATION RATES IN AIR

By

Justin K. Smith

B.S, Electrical Engineering, University of New Mexico, 2017

M.S, Electrical Engineering, University of New Mexico, 2019

ABSTRACT

The ionization of gas molecules from the absorption of photons produced in different parts of a discharge is an important process in the development of streamers. Photoionization rates are essential in the propagation of streamers and are therefore important in simulations of computational codes. Although streamers are widely used in computational codes, there is a limited data set on the experiments measuring photoionization rates in gases. Usually, the photoionization rate data used in computational codes comes from a single source and the validity of this data combined with the photoionization model has been questionable. It is postulated there is a probable uncertainty in photoionization rates as high as a factor of four. To improve the current state of the art simulations, an experimental setup capable of measuring photoionization produced from a gas discharge provides new photoionization data.

TABLE OF CONTENTS

LIST OF FIGURES

LIST OF TABLES

Chapter 1

Introduction

1.1 Background

When a high voltage is present in a neutral gas, the gas can ionize forming a conductive channel that can carry current, which is known as electrical breakdown of gases. Two primary ways of forming a conductive channel are the Townsend discharge and the streamer mechanism. The Townsend discharge occurs in a uniform electric field and the streamer mechanism forms in a non-uniform electric field. The streamer mechanism is important for many reasons because they can occur naturally like in sprites above the atmosphere [1] or from high voltage pulses applied to a gap [2-5].

During the development of streamers, Ultraviolet (UV) photons are produced from different parts of the discharge and these photons are absorbed by molecules leading to ionization of the gas in a process called photoionization. It is generally accepted that in air, the dominant source of UV photons comes from radiative transitions from N_2 singlet states of $b^1\Pi_u$, $b'^1\Sigma_u^+$ and $c_4'^1\Sigma_u^+$ [6] that are capable of photoionizing O_2. This plays a critical role in the propagation of streamers since free electrons are created in front of the streamer head as shown in figure 1.1. Accordingly, the photoionization rate is important in plasma codes to simulate streamer propagation and there is an increasing demand for photoionization rates [7]. However, there is a limited data set on the experimental measurement of photoionization rates in gases [8-11].

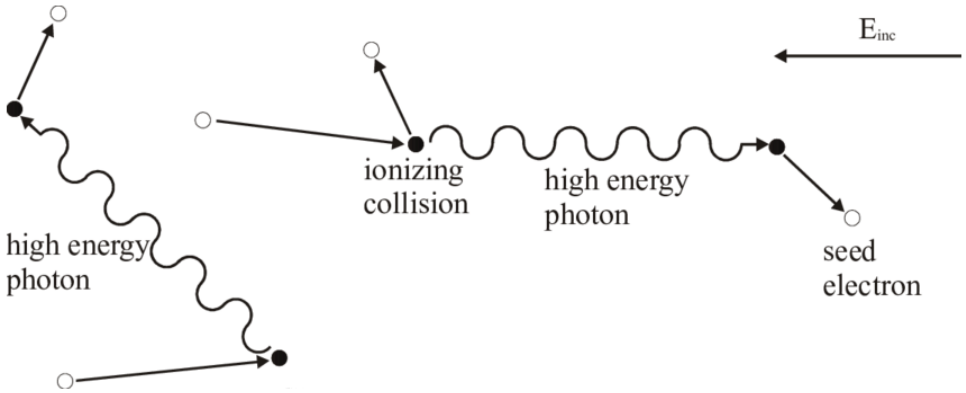

Figure 1.1: Propagation of a streamer from photoionization

In the fluid approach of modelling streamers, the electron and ion dynamics are governed by the continuity equations. To take into account photoionization rates, a source term is added to the continuity equations for both electrons and ions. In the literature, this photoionization source term consists of the experimental data of [10] and the photoionization model proposed by [6] given by

$$Q_\phi = \int_{V_1} dV_1 \, \alpha v_d n_e \int_{\Omega} d\Omega \, R_2(\Omega) \int_{R_1(\Omega)}^{R_2(\Omega)} dr \frac{\psi}{4\pi} \frac{p_q}{p_q + p} \tag{1.1}$$

$$\psi = \frac{\omega}{\alpha} \xi f \tag{1.2}$$

$$f = \frac{e^{(-k_{min} pr)} - e^{(-k_{max} pr)}}{r ln(k_{max}/k_{min})} \tag{1.3}$$

The variables used in these equations are listed and defined in table 1.1.

Variable	Variable Definition
$\boldsymbol{v_d}$	Electron Drift velocity
$\boldsymbol{n_e}$	Electron density
$\boldsymbol{\Omega}$	Solid angle
$\boldsymbol{\psi}$	Photoionization coefficient function
$\mathbf{p}$	Pressure
$\boldsymbol{p_q}$	Quenching pressure
$\boldsymbol{\omega}$	Excitation of emitting states coefficient
$\boldsymbol{\alpha}$	First Townsend ionization coefficient
ξ	Photoionization efficiency
$\boldsymbol{k_{min}}$	Miniumum absorption coefficient
$\boldsymbol{k_{max}}$	Maximum absorption coefficient
$\boldsymbol{V_{1,2}}$	Volumes 1 and 2
$\boldsymbol{R_{1,2}}$	Distance connecting volumes 1 and 2

Table 1.1 List of variables and definitions

The source term is calculated using the integral representation given in equation 1.1 [1, 4, 12 13] for a given point of the volume where the discharge occurs making this method computationally expensive. Improvements of the photoionization source is done by using a set of differential Helmholtz approximation for the absorption function [14-17] that reduces the time spent on calculating the photoionization source term. One important remark to make is the model has to be fit to the data used in a simulation. In the literature, it is common to vary the parameter $\xi \frac{\omega}{\alpha}$ as a scaling factor in order to fit the data. The parameter $\xi \frac{\omega}{\alpha}$ describes the radiation characteristics of the source and changing this value

has an impact on the photoionization rate. Values of $\xi \frac{\omega}{\alpha}$ are taken from the literature and shown in table 1.2.

Reference	Value of $\xi \frac{\omega}{\alpha}$
Kulikovsky [12]	0.1
Naidis [18]	0.03
Bourdon [15]	0.06
Bagheri [17]	0.075, 0.0375, 0.15

Table 1.2: Different values of $\xi \frac{\omega}{\alpha}$ used in simulations taken from literature

There have been some concerns on the reliability of the photoionization model [5, 13] based on Zheleznyak [6] and Penney & Hummert [10] data at higher pressures. Naidis [18] performed a simulation based on equations 1.1, and 1.2 using the experimental data of [9] and [10] and found a difference of about a factor of two between the two data sets. Naidis [18] attributed this difference to the quenching of radiative states of N_2 where quenching effects are important at atmospheric pressures that were proposed by Teich [9]. Nudnova [4] gives an uncertainty of photoionization to be as high as a factor of four. A factor of two is given by the results of Naidis [18] and the other factor of two comes from the analysis of Zheleznyak [6]. In the derivation of the model, the coefficient $\xi \frac{\omega}{\alpha}$ is a parameter that depends on E/p, where E is the electric field and p is the pressure. The value of the coefficient ranges between 0.12-0.06 based on the reported values for E/p in [8]. Combining this variation with the difference of magnitude between atmospheric and low pressure, gives an overall factor of four.

This factor can have a huge impact on the results of simulations involving streamers and may lead to inaccurate results. Therefore, the purpose of this experiment is to improve the current state-of-art streamer simulations by producing more accurate photoionization rate data. The pressure range of range of the measurements start at the Penney & Hummert [10] range of 0.3-17.5 Torr in air. The measurements will be compared with the results of Penney & Hummert [10] and the model proposed by Zheleznyak [6] to validate this model with new photoionization data.

Chapter 2

Theoretical Background

To gain a better understanding of the processes involved in photoionization, it is beneficial to review the fundamental mechanisms that are involved. An overview of the basics of a gas discharge is presented along with a brief overview of the spectral physics involved since this is responsible for the generation of photons. There is an abundance of literature on gas discharges and spectral physics [19-24]. The following sections describe the mechanisms behind an electrical gas and the types of discharges that can occur. The last sections describe the excitation and emission processes of molecules from one electronic state to another.

2.1 Electrical Breakdown

Electrical breakdown refers to the process of changing the properties of a gas from a good insulator to a good conductor, which allows a current to flow through it. Electrical breakdown can happen in two cases: 1) a uniform electric field and 2) a non-uniform electric field. These mechanisms will be discussed below starting with the uniform field.

2.1.1 Electron Avalanche

An electron avalanche forms when any free electrons present are accelerated by an applied electric field, collides with the background gas, and ionizes creating new electrons as shown in figure 2.1.

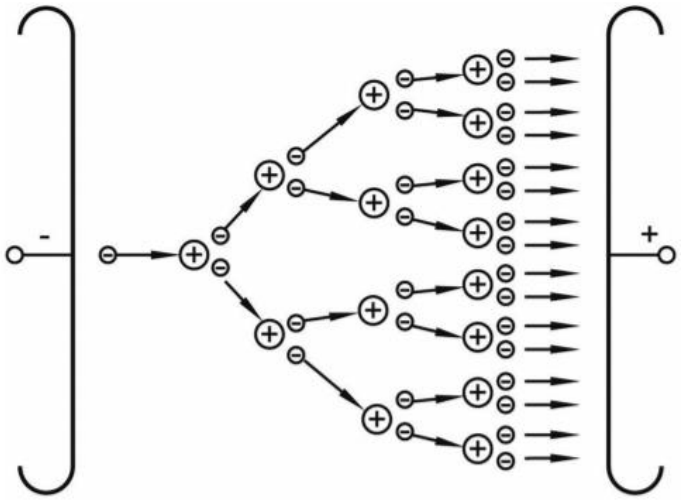

Figure 2.1: Electron avalanche initiated from a single electron [19]

These newly created electrons gain energy through the applied electric field and further ionize the gas and continues to create electrons at an exponential rate. The number of electrons that reach the anode some distance away is:

$$n(d) = n_0 e^{\alpha d} \tag{2. 1}$$

where n_0 is the initial electron density, d is the distance away from the initiation point of the avalanche, and α is the first Townsend ionization coefficient which describes the number of electrons created per unit length.

2.1.2 Townsend Mechanism

The Townsend mechanism is a form of electrical breakdown that develops in a uniform electric field that forms from multiple electron avalanches rather than a single electron avalanche since a single electron avalanche cannot carry the full breakdown current. Starting with the initial electron avalanche, a secondary mechanism to generate more electron avalanches occurs when the ions from the initial avalanche bombard the cathode releasing more electrons called secondary electrons. As each electron leaves the cathode,

they create $\gamma \cdot (e^{\alpha d} - 1)$ electrons from collisions with the surrounding gas. γ is a coefficient that determines the number of secondary electrons emitted from the cathode. The number of electrons reaching the anode is

$$n(d) = \frac{n_0 e^{\alpha d}}{1 - \gamma \cdot (e^{\alpha d} - 1)} \tag{2.3}$$

from equation 2.3, the current produced from these electron avalanches is

$$i = \frac{i_0 e^{\alpha d}}{1 - \gamma \cdot (e^{\alpha d} - 1)} \tag{2.4}$$

which is known as the Townsend Discharge that describes the current growth or electron growth of a gas.

2.1.3 Streamer Mechanism

The Townsend mechanism describes how a conducting channel forms from one electrode to the other from an avalanche but a problem with this mechanism occurs with large gaps and/or higher pressures. The time of the conducting channel to reach from one electrode to the other is dependent on the ion drift velocity. At these elevated pressures and gap distances, the ion drift velocity is too slow to create this conducting channel, which often travels on a timescale of $\sim 10^8\ cm/s$. During this time, photons are capable of travelling the gap length and are responsible for creating the free electrons needed to create a conducting channel. This conducting channel is often thin and grows fast from one electrode to the other, which is referred to as a streamer.

A streamer can come in two types: a cathode-directed (positive) streamer and an anode-directed (negative) streamer with the former relevant to this investigation. Figure 2.2 shows the formation and propagation of a positive streamer.

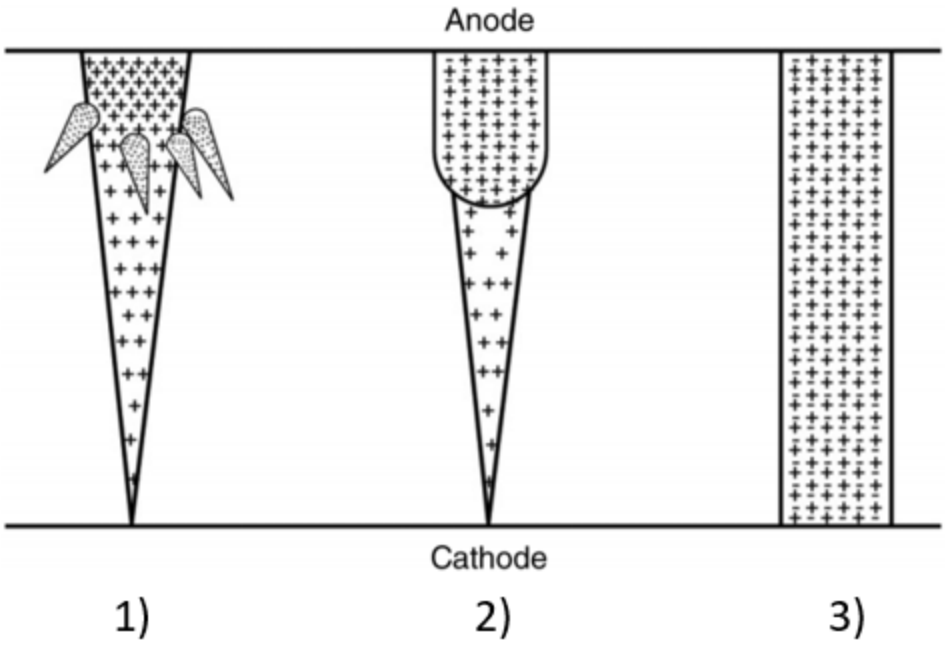

Figure 2.2: Formation and propagation of a positive streamer [20]

In region 1), the electron avalanche traverses the entire gap from the cathode to the anode leaving a trail of ions that grows more towards the anode. Near the anode region, high-energy photons create additional avalanches. In region 2), a region of space charge accumulates and starts to grow larger due to diffusion. More high-energy photons are created near the head of the space charge allowing the streamer head to grow and propagate. In region 3), the streamer traverses the entire gap and full breakdown occurs.

2.1.4 Corona Discharge

In a non-uniform field, the electric field produces a localized discharge near regions where the strength of the electric field gradient is high. The electric field strength decreases the further away from the electrode that does not allow for full breakdown, which confines the discharge to remain near the electrode. A discharge that forms in this way near sharp points or sharp edges that greatly increases the field strength is called a corona discharge.

Corona is characterized by a luminous glow around the high electric field. Corona is also an audible discharge that produces a hissing noise and the intensity of the hissing sound increases with voltage. A corona discharge can exist in two forms depending on the polarity of the electric field, which are a positive corona discharge and a negative discharge. When a positive voltage is applied to the cathode, the strong electric field gradient initiates an electron avalanche.

2.2 Excitation and Ionization Processes

During the breakdown of a gas, there are different types of ionization and excitation processes that occur during this time and is shown in table 2.1. The interaction of the free electrons from the discharge with the molecules is of importance since one the processes is responsible for producing UV photons. The free electrons gain energy from the applied electric field and collide with a neutral molecule. This collision gives energy to the molecule and causes the valence electron to jump to a higher energy state, which is known as electron impact excitation.

When a photon is emitted from a molecule, the photon interacts with another molecule. The molecule absorbs the photon and one of two things can happen. The electron of the molecule jumps to a higher energy, which in this case is another excitation. Alternatively, if the photon has an energy greater than the ionization potential of that molecule, then the electron is removed from the molecule and results in an ionized molecule from a process called photoionization.

Reaction	Result
$A + e \rightarrow A^* + e$	Electron impact excitation
$A^* + e \rightarrow A + h\nu + e$	De-excitation from electron
$A^* + B \rightarrow A + B$	De-excitation from another molecule
$A + h\nu \rightarrow A^+ + e$	Photoionization

Table 2.1: A and B are molecules, A^* is an excited molecule, e is an electron, h is Planck's constant, ν is the frequency of the photon

2.3 Physics of Excited States

Since photoionization in electrical discharges, rely on UV photons produced from excited states of the molecules in the gas, it is useful to have an understanding of the basics involved in determining the notation, excitation, and emission processes of these excited states.

2.3.1 Term Symbol

Any molecule can have a number of different electronic states that can occur and it is helpful to have a way of classifying these electronic states. These electronic states represent the different potential energy curves and in the case of photoionization, it is important to know which of these states can emit UV photons. The term symbol is used as a shorthand notation to describe these electronic states and is given by:

$$^{2S+1}\Lambda^{\pm}_{g,u} \tag{2.5}$$

where (2S+1) refers to the multiplicity, Λ is the total angular momentum quantum number that is a linear combination of atomic orbitals, $\pm$ is the symmetry of the orbital upon reflection, and (g,u) refers to the parity of the molecule.

The quantum number (Λ) is composed of the orbital angular momentum of the electrons orbiting around the molecular axis. For a particular configuration, the possible values of Λ can be $\Lambda = |M_L|$, where M_L is the individual electron orbital angular momentum. Each molecular energy state will have a term symbol associated with the value of Λ given by the conventional scheme shown in table 2.2.

Λ:	**0**	**1**	**2**	**3**	**…**
Term symbol:	Σ	Π	Δ	Φ	…

Table 2.2: Term symbol classification

In the multiplicity term, (2S+1), S is the quantum number of the sum of the individual electron spins. Depending on the total number of electrons, S can take integral or half-integral numbers. With different values of S, the multiplicity can take different values as well and determines the spin states the electrons can be in as shown in table 2.3.

Spin State	**Multiplicity (2S+1)**	**Quantum Spin Number S**
Singlet	1	0
Doublet	2	$\frac{1}{2}$
Triplet	3	1

Table 2.3: Multiplicities from the total spin number

In the case of a singlet state all of the electrons are paired according to their spin, for example spin up-spin down. A doublet state has one unpaired electron that can have two different states it can be in; the electron can have a spin up or a spin down. A triplet state has two unpaired electrons that can give three different configurations the electrons can have. Both the electrons can a spin up, spin up spin down, and spin down spin down pairing.

For a homonuclear diatomic molecule, a molecule that has two of the same molecules, there is a center of symmetry between the two molecules. When an inversion through the center of the two molecules occurs, the wavefunction of the electrons can change sign or remain the same. If the sign changes, then the wavefunction is antisymmetric which is given the German term ungerade (u) for odd parity shown in figure 2.3. If the wavefunction retains its symmetry, then it is called gerade (g) for even parity shown in figure 2.4.

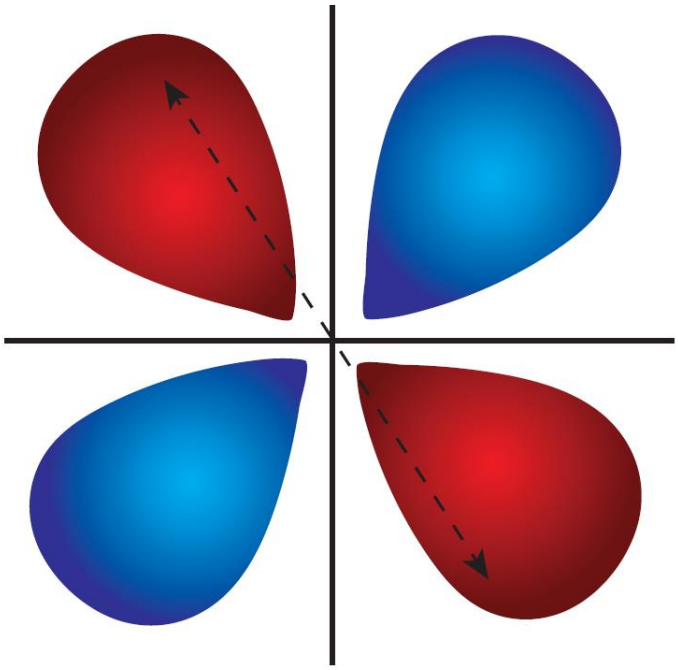

Figure 2.3: Even parity of an orbital through center of inversion

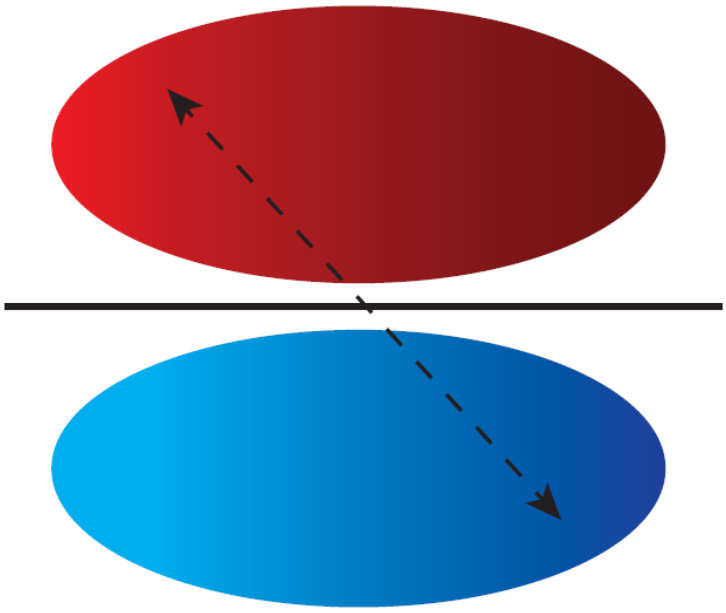

Figure 2.4: Odd parity of an orbital through center of inversion

In the definition of Λ, if the value of M_L is zero, the term symbol was designated by the Σ state. If the value of M_L is non-zero then the higher molecular states, Π, Δ, Φ, … will have two possible values for each of them. These two values are called doubly degenerate states. If a plane is taken through the molecular axis to form a plane of symmetry, the electronic wavefunctions will either retain the same sign or change sign when reflected through this plane. In the case of the doubly degenerate states, a reflection on the plane of symmetry can change the sign of the wavefunction but the two values of the state will have exactly the same energy. For these states, classifying the reflection is not necessary. However, for Σ states, the electronic wavefunction will change sign upon reflection since there is only one value of M_L making it a non-degenerate state. If the sign of the wavefunction remains unchanged, this is designated with a + in the term symbol as Σ^+. If the sign of the wavefunction changes, this is given a – in the term symbol as Σ^-.

With the molecular term symbol defined, one more classification is needed when describing any molecular electronic state. In front of the term symbol is usually a letter describing the energy level of the given state. The ground state of any molecule is given the letter X in front of the term symbol. Higher molecular states with the energy increasing with the letters, A, B, C, …. One important distinction needs to be made when comparing the multiplicity of each state. If the multiplicity of any higher electronic state matches with the ground state, then that state with have a capital letter associated with it. If the multiplicities are different, a lower-case letter is given instead of a capital letter. Examples of term symbols with the labeling of the letters for N_2 is shown in figure 2.5.

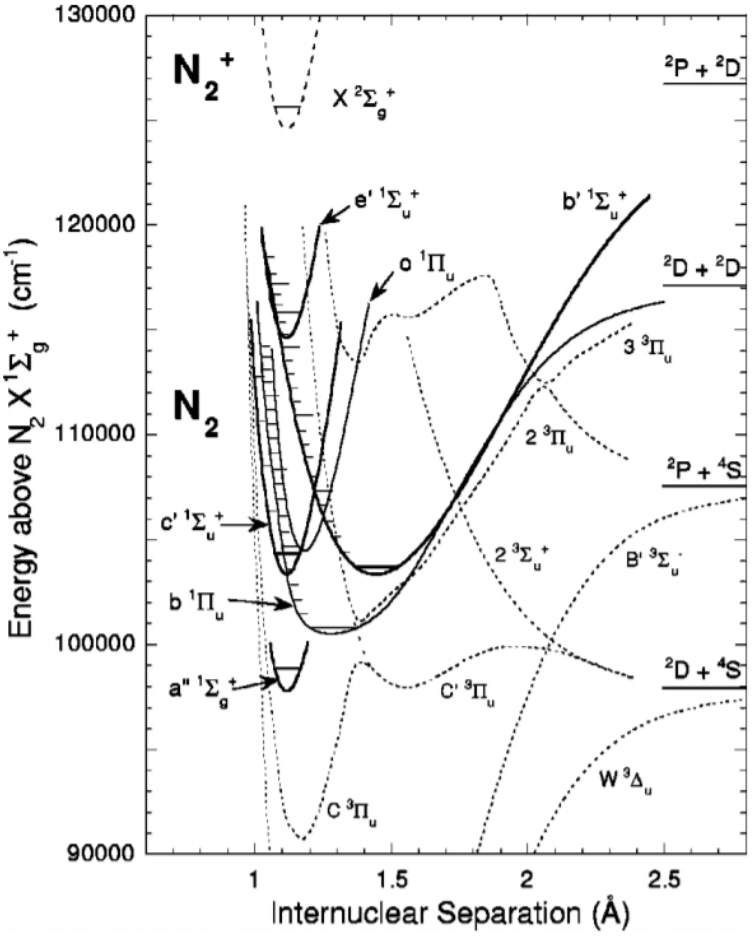

Figure 2.5: Potential energy curves of N_2 with term symbols [25]

2.3.2 Boltzmann Distribution

For any given molecule, there are a number of excited states that can be populated from an excitation event. However, not all of the molecules will become excited and only portion can be excited. To describe the photon emission and absorption processes of molecules, the population of molecules at a particular state needs to be known. If the system can be considered in thermal equilibrium, that is the temperature of the system can be characterized by one value, then the probability of finding molecules at a given excited state relative to another state is described by the Boltzmann Distribution equation

$$N_j = \frac{N g_j}{Q(T)} e^{-E_j/k_b T} \tag{2. 2}$$

where N_j is the population density of molecules in state j, N is the total population density of molecules, E_j is the energy of the jth level, k_b is Boltzmann's constant, g_j is the statistical weight that takes into account the degeneracy of state j, and Q(T) is the partition function that sums all possible ways a molecule can distribute electrons:

$$Q(T) = \sum_{j=0}^{\infty} g_j e^{-E_j/k_b T} \tag{2. 3}$$

Based on equation 2.3, as the temperature increases, the likelihood of finding a large population of molecules decreases and majority are at the ground state.

2.3.4 Spontaneous Emission

The interaction of a photon with molecules occurs through three different processes called, spontaneous emission, stimulated emission and stimulated absorption. Only spontaneous emission is considered in this experiment. If a population of molecules in an

excited state m transitions to a lower state n, a photon is emitted with an energy with the difference between these states. However, not all of these transitions will emit a photon so there is a probability of states emitting a photon. This transition probability is called the Einstein coefficient for spontaneous emission, A_{mn}, that gives the probability per second that a molecule will emit a photon. The general definition of A_{mn} is given by

$$A_{mn} = \frac{64\pi^4 {\nu_{mn}}^3}{3h} |R_{mn}|^2 \tag{2.4}$$

where $|R_{mn}|^2$ is the transition electric dipole moment that depend on the initial and final wavefunctions of the molecule. In the definition of the molecular term symbol in section 2.3.1, the definition of the parity of a molecule determines the value of $|R_{mn}|^2$. A transition between two states with even parity has no net dipole and no photons are emitted. A transition between an even and odd parity will emit a photon.

Chapter 3

3.1 Experimental Setup

An experimental setup was designed to measure the amount of photoionization created from a low current corona discharge at various pressures, and distances. The experimental setup shown below in figure 3.1 consists of a source chamber that is responsible for creating the UV photons and a collector chamber where the measurement of photoionization occurs. The source chamber has a 2-3/4" Conflat (CF) glass viewport to view the corona discharge from a point electrode. The source chamber has ports for the vacuum pump and pressure monitor. The end of the source section has a solid copper gasket with a 4 mm hole drilled through to allow a portion of the radiation to pass through into the collector chamber. The collector chamber consists of a 3D printed collector electrode, gas injection system, and a port for current measurement. Figure 3.2 is schematic of the inside of the chamber and how the instruments are used. All of these components will be discussed in the following sections.

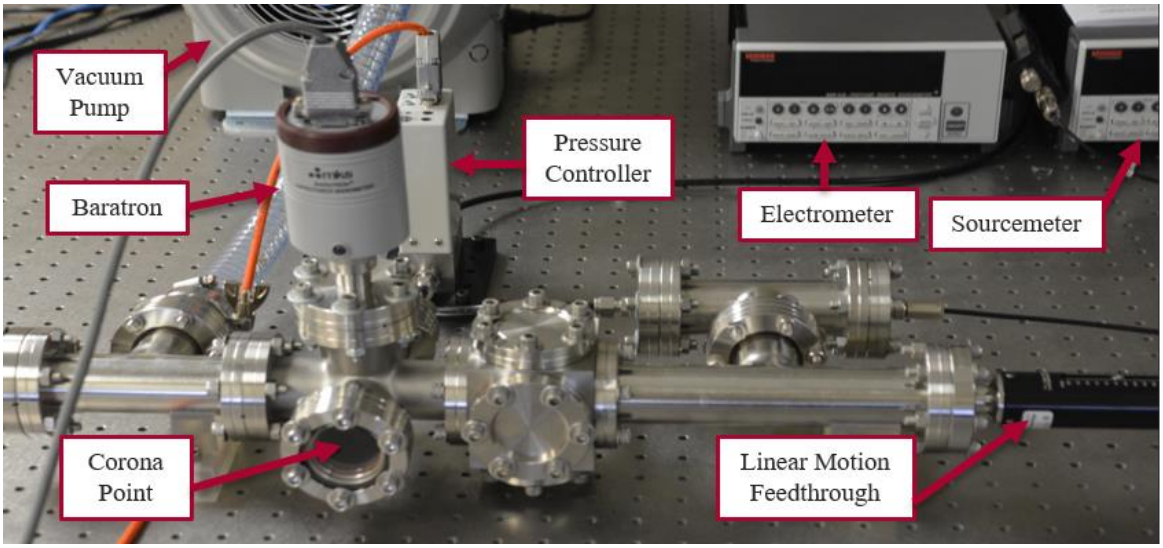

Figure 3.1: Experimental setup

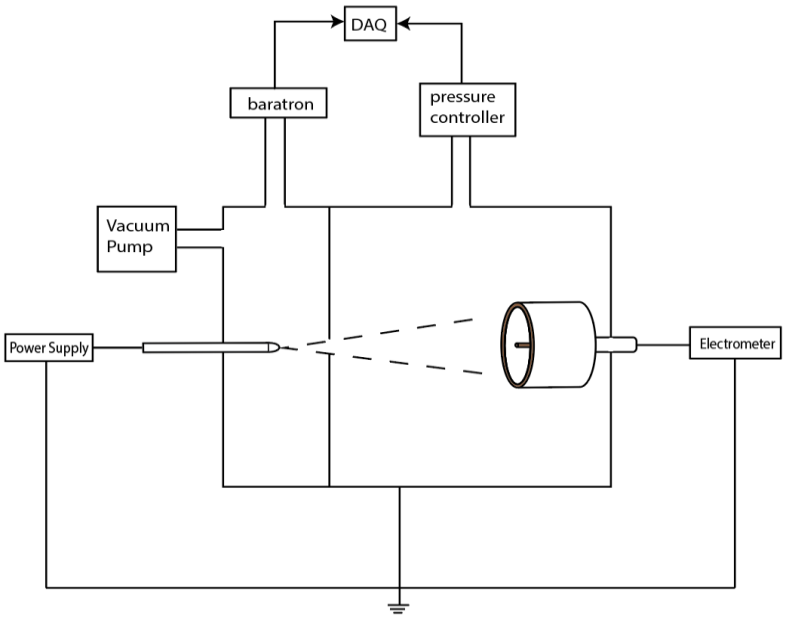

Figure 3.2: Schematic of experimental with the labeling of instruments

3.1.1 Electrode

The electrode to create the corona discharge is done by using a 1/16” tungsten-welding electrode sharpened to a point. Tungsten was chosen since it is a rather hard metal that when sharpened, retains a sharp point. To sharpen the tungsten electrode, a Dremel with a welding electrode sharpener was used. The electrode is sharpened at an angle and the measurements are shown in figure 3.3. Sharpening the electrode at an angle to make a point creates a highly non-uniform electric field that generates a corona discharge easily.

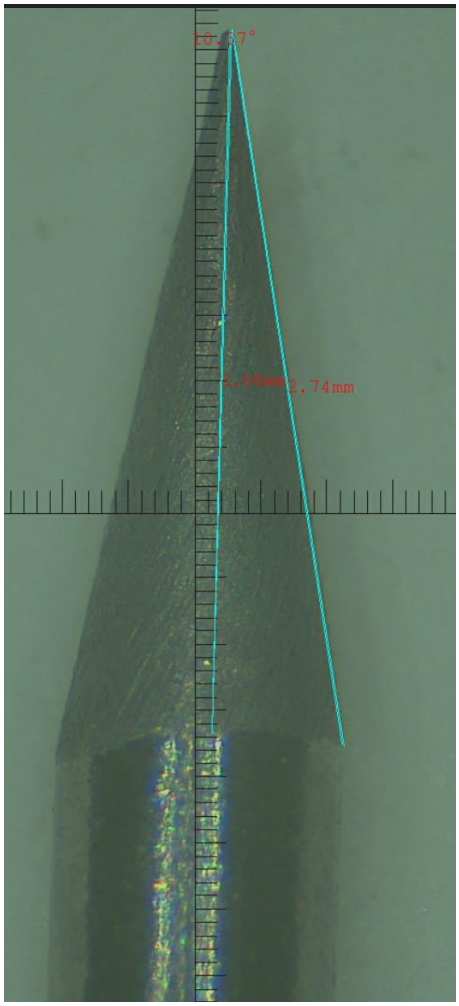

Figure 3.3: Electrode tip with dimensions

To mount the electrode inside the vacuum chamber, a piece of 3/8” brass rod with rounded edges is drilled slightly larger than the tungsten electrode. The tungsten electrode is inserted into the brass piece and the brass rod is heated to expand while tungsten electrode is inserted. Once the brass rod cools, the tungsten rod is tightly fit inside the brass piece. Both of these pieces are then mounted on an isolated copper feedthrough.

3.1.2 Collector

To measure the amount of photoionization produced in the chamber, a custom 3D printed collector was designed to hold two conductors and is shown in figure 3.4. The

collector was 3D printed using a Formlabs Form 2 printed constructed out the rigid resign to provide durability. The thickness of the collector is 0.254 cm thick and a diameter of 1.9304 cm. The outer conductor is a hollow copper cylinder with a diameter of 1.8 cm and a thickness of 0.45 mm. The inner conductor is a single stranded copper wire with a diameter of 0.2032 cm.

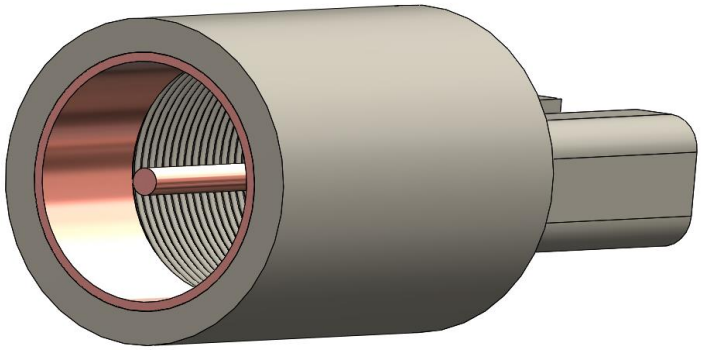

Figure 3.4: SolidWorks model of the collector used

The back of the collector extends back one inch with a width of 0.25 inches to mount onto a linear motion feedthrough. This allows the distance between the collector and the pin electrode to vary which changes the photoionization. A voltage is applied to the inner and outer conductors to attract the electrons and ions produced from photoionization that generates a measured current. The photoionization current varies in the range of pA ($10^{-12}\ A$) to fA ($10^{-15}\ A$). To be able to measure this low of current, the entire collector is surrounded with an additional conductor to use a technique called active guarding, which will be discussed in a later section.

3.1.3 Power Supplies

The Tungsten pin was biased by a Keithley 2410 Source Measure Unit (SMU), shown in figure 3.5, that can provide up to a maximum voltage of 1.1 kV and up to a maximum

current of 1 A. An SMU is an instrument that can simultaneously source a voltage/current and measure a voltage/current precisely giving highly accurate measurements. This gives an advantage of using only one instrument to source and measure, reducing the amount of time between remotely programming the instrument and recording measurements. Each current measurement can have up to six and half digits of precision meaning six digits of accuracy and the last digit is rounded up. Table 3.1 shows some measurement accuracies based on the range of interest and source current values. In this experiment, the corona current was in the range 0-50 µA and have the measurement accuracies shown in table 3.1.

Figure 3.5: Keithley 2410 SMU

Range	Source Current	Accuracy
1µA	1.00000 µA	0.059%
100 µA	100.000 µA	0.031%
1 mA	1.00000 mA	0.033%

Table 3.1: Measurement accuracies of Keithley 2410 for different current ranges [26]

The collector was biased with a Keithley 6430 Sub-femptoamp SMU that can provide a maximum voltage of 200V and maximum current of 100 mA shown in figure 3.6. The 6430 functions in the same way as the 2410 with the exception that it can measure extremely low current values. Since the typical current range of photoionization is between pA and fA, the 6430 provides very accurate measurements in this range and has a maximum resolution of 10 aA ($10^{-18}A$) as shown in table 3.2. To get the current measurement this small from inside the chamber to the 6430 without losing any signal, the active guarding technique is used and is discussed in the following section.

Figure 3.6: Keithley 6430 SMU Sub-femptoamp Electrometer

Range	Resolution	Accuracy
1 pA	10 aA	1%
1nA	10 fA	0.05%
1µA	10 pA	0.05%

Table 3.2: Measurement accuracies of Keithley 6430 for different current ranges [27]

3.1.4 Active Guarding

Whenever a low current measurement is performed, there is a high chance the measurement can become affected by a leakage current. A coaxial cable has an inner and outer conductor separated by an insulating material. If a voltage is applied to the inner conductor, there is a small current that leaks through the insulating material. Typically, this leakage is often in the nA range which means if the current measurement of interest should be in the pA range, the measured signal is just the leakage current as shown in figure 3.7.

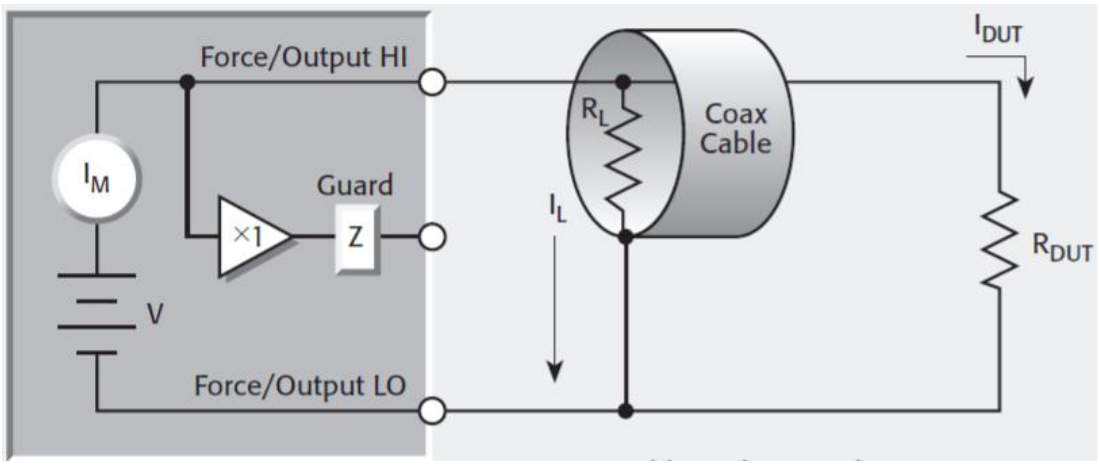

Figure 3.7: Unguarded Circuit using coaxial cable, without guard connection [28]

Guarding is a very effective way of reducing the impact of leakage current on a measurement. To use guarding for a low current measurement, a triaxial cable is used in place of a coaxial cable. A triaxial cable consists of an inner conductor, a shield or guard conductor, and an outer conductor separated by insulating material. The inner shield is driven by a unity gain amplifier, that gives the inner shield the same voltage that is on the inner conductor. The voltage difference between the inner conductor and shield is essentially zero and the leakage current is eliminated and is shown in figure 3.8.

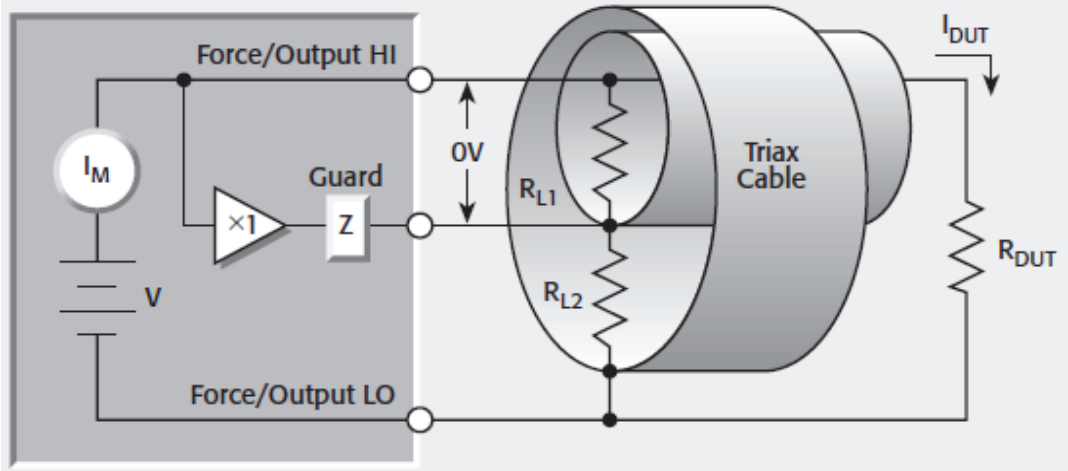

Figure 3.8: Guarded Circuit using a triaxial cable with guard connection [28]

In this experiment, the active guarding technique is applied to the collector the inner conductor and outer conductor are connected to the inner and outer conductor of the triaxial cable. As mentioned in section 3.1.2, the collector is covered with an additional conductor that is connected to the shield of the triaxial cable. The photoionization current can now be measured without any leakage current affecting the measurement.

3.1.5 Pressure System

A 1000 Torr 640B MKS Instruments pressure controller, figure 3.9, is used to control the pressure inside the vacuum chamber. The 640B has a flow rate of 5000 sccm with a control accuracy of $\pm$2 Torr and a measurement accuracy of $\pm$0.5%. On the source side of the chamber, an Absolute 100 Torr 626C MKS Instruments Capacitance Baratron Manometer, figure 3.10, monitors the pressure of the corona discharge. The pressure readings have an accuracy of 0.25% of the reading and has a resolution of 0.001 Torr.

Figure 3.9: MKS Instruments 640B pressure controller

Figure 3.10: MKS Instruments 626C Baratron Capacitance Manometer

Both the 640B pressure controller and 626C baratron have a 15-pin D-sub connector that can control and read measurements from these devices. A National Instruments (NI)

USB-6001 multifunction Data Acquisition (DAQ), figure 3.11, reads and controls both devices. The USB-6001 DAQ allows multiple analog inputs with a voltage range of ± 10 V and the inputs can be single-ended or differential. The USB-6001 also has two analog outputs with an output range of ± 10 V. The USB-6001 has a 14-bit Digital-to-Analog (DAC) converter that is used to generate the analog output voltages and the increments can be as small as 1.22 mV. The ability of outputting an analog voltage of 10V allows the DAQ full control the 640B pressure controller and can be set to any desired pressure.

Figure 3.11: National Instruments USB-6001 DAQ

3.1.6 Vacuum Pump

To remove the initial gas inside of the chambers, a dry scroll Agilent IDP-15 vacuum pump, shown in figure 3.12, can bring the base pressure inside to 10 mTorr. The dry scroll pump was chosen since it operates without any oil compared to other available pumps. With standard oil pumps, there is a possibility that oil can leak into the chamber due to negative pressure if the pump turns off. With a dry scroll pump, the vacuum pump operates with air which prevents any contamination inside the chamber. The vacuum pump can achieve a peak pumping speed of 256 L/m which is more than enough of a pumping speed

for this experiment. Since there is a small aperture separating the two chambers, there is a pressure differential across that interface. The high pumping speed helps maintain a low pressure in the source chamber as the pressure in the collector chamber increase.

Figure 3.12: Agilent IDP-15 Dry scroll pump

3.1.7 Linear Motion Feedthrough

To vary the distance between the collector and pin electrode, the collector is mounted onto a Huntington Vacuum Linear Motion Feedthrough shown in figure 3.13. When the feedthrough is set to be at zero on the dial, the collector is 13 cm away from the pin electrode. The maximum distance away the collector can be when the feedthrough is maxed out is 5 cm where the collector would be at 18 cm away. The feedthrough can be precisely adjusted with a resolution of 0.2 mm.

Figure 3.13: Huntington Vacuum Linear Motion Feedthrough L-2111-2-A

3.2 Data Collection and Analysis

A LabVIEW program was created to control the instruments and to collect data from the 2410 Sourcemeter and 6430 Electrometer. In order to control and receive data from the 2410 and 6430, a GPIB cable is used as an interface between LabVIEW and the instruments as shown in figure 3.14. In the main Virtual Instruments (VI), Keithley drivers for both the 2410 and 6430 are used to set the voltage, current compliance levels and measurement settings. The data collection part of LabVIEW combines the measurement readings from the 2410 and 6430 with the pressure readings and combines it into a text file. This text file is read into MATLAB for data analysis.

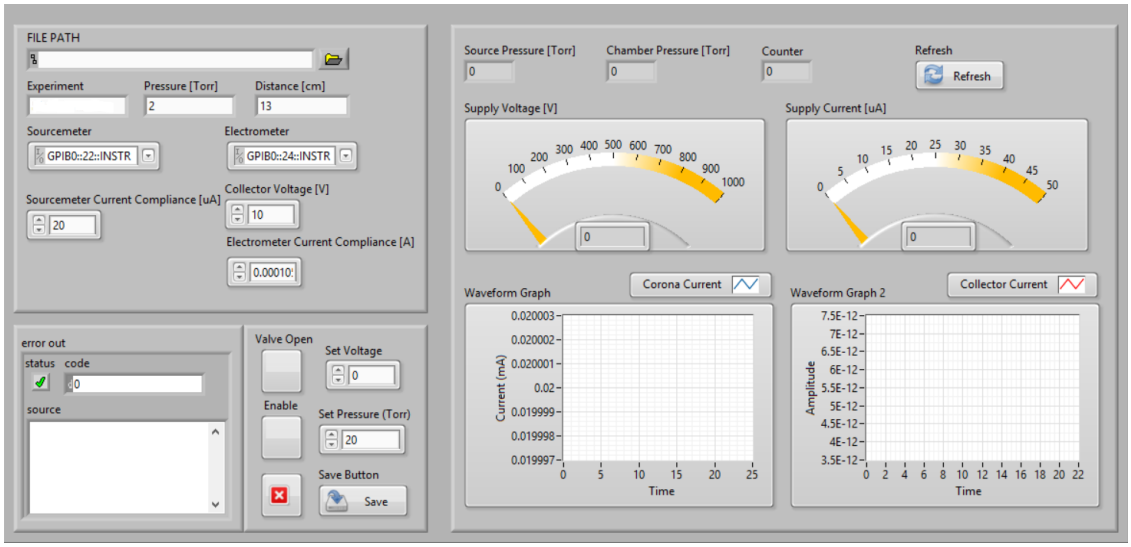

Figure 3.14: LabVIEW front panel

A MATLAB script was written to process the data from LabVIEW. The script first opens the text files generated by LabVIEW. Then MATLAB opens each of the text files and extracts the corona current, collector current, pressure, and distance away from the discharge. MATLAB plots the photoionization coefficient in the same way defined in [10] as

$$\psi = \frac{i_c}{i_d p d \theta} \tag{3.1}$$

where i_c is the collector current, i_d is the corona current, p is the pressure, d is the depth of the collector and θ is the solid angle of radiation that passes through to the collector chamber. A sketch of how these variables are laid out in the experimental setup is shown in figure 3.15

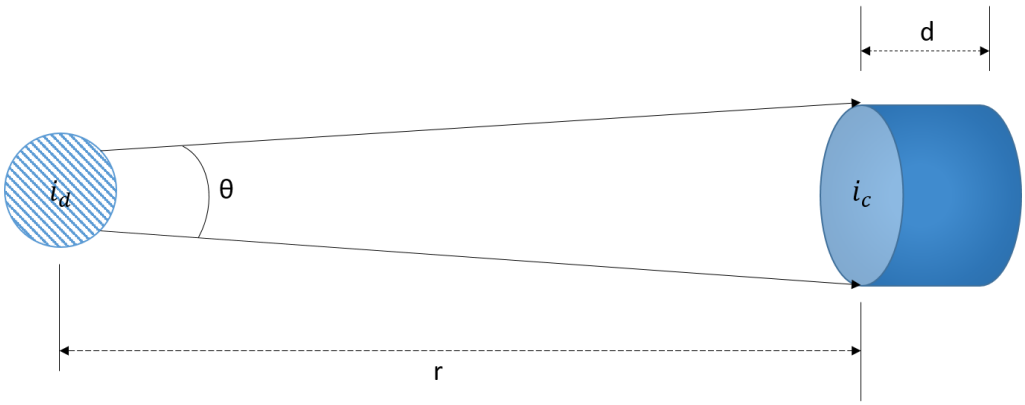

Figure 3.15: Diagram of experimental measurements

3.3 Measurement Procedure

The collection of photoionization data was done with the following procedure. The vacuum chamber was first pumped down to a minimum pressure of 0.23 Torr. Then using the pressure controller, the pressure inside the vacuum is set at a desired constant pressure. Once the pressure was set, a voltage is applied to the electrode to generate a corona. At the same time, the 2410 measures the corona current. The 6430 measures the resulting collector current simultaneously. Once those measurements are made, the voltages goes to zero and the collector distance is adjusted with the linear feedthrough. Then the process repeats for the desired number of data points to collect.

Chapter 4

Results

The results presented in this section is in the low-pressure range of 0 - 17.5 Torr where any quenching effects are negligible. The experimental data will be compared against the Penney & Hummert data set for air [10] and the model of Zheleznyak [6] based on the experimental procedure discussed in section 3.3.

4.1 Experimental Results

The measured values of this experiment is plotted in the same respect as the Penney & Hummert [10] data set. The x-axis represents the product pr, which is a product that is proportional to the number of molecules at a given length a photon could interact with. The y-axis is the logarithmic photoionization coefficient used in [10] defined as the number of photoionized ions generated per ions formed in the discharge. Figure 4.1 shows the results of photoionization from a 20 μA corona discharge and measured at distances of 13-18 cm away. A total of 10 pressure values starting at 0.3 up to 17.5 measured at distances of 13-18 cm for each pressure value.

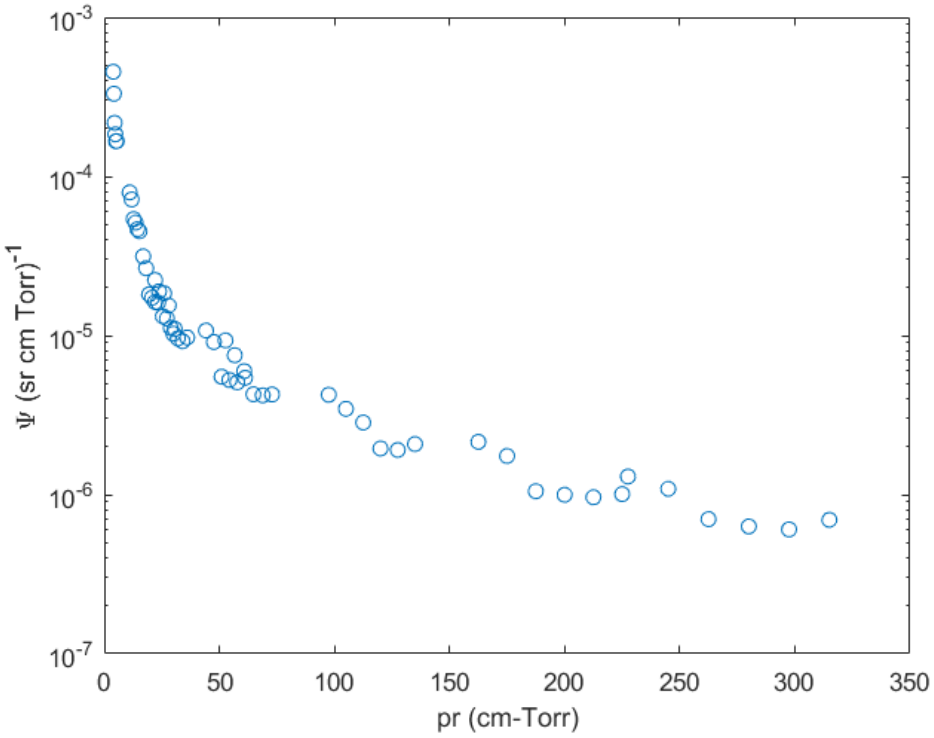

Figure 4.1: Measured photoionization data

The data in figure 4.2 tests the repeatability of the measurements given identical conditions as the data in figure 4.1. Figure 4.2 shows the results of the second experiment overlaid with the first data set. Comparing the two data sets, there is some variation between the two but the deviation is not drastic. This gives confidence that photoionization is what is being measured and not something else like noise for instance.

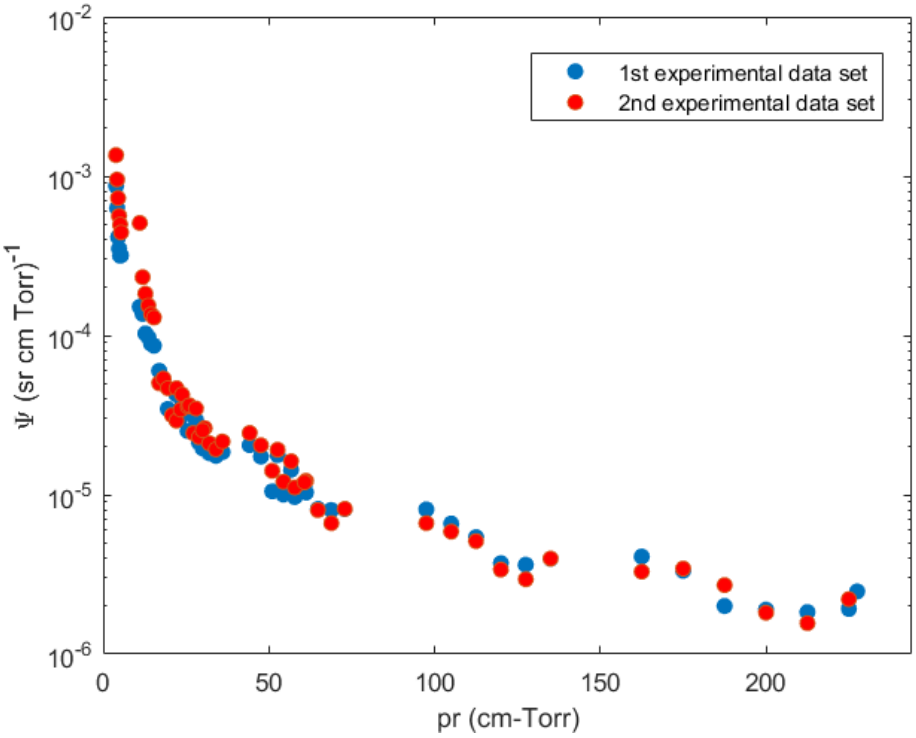

Figure 4.2: Repeatability of Ψ measurements

A series of measurements were performed that are slightly different than the experimental procedure described in section 3.3. Instead of keeping the pressure constant and varying the distance, the distance was held constant in these measurements and the pressure was varied. Since the photoionization coefficient is plotted against the parameter pr, then the measurements should yield the same results regardless of how they were made. Figure 4.3 shows the results of a series of five measurements that start from a distance of 14 cm to 18 cm in 1 cm increments while varying the pressure in each case. Although there is some separation between the measurements, they all have the same shape and fit closely together.

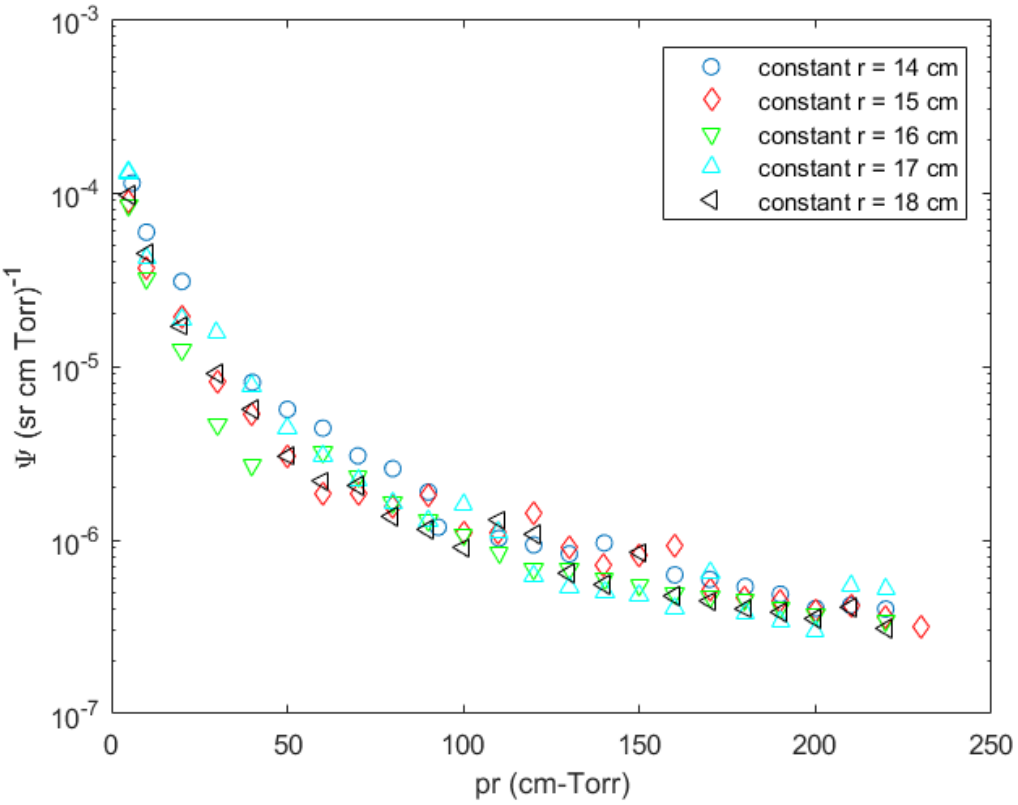

Figure 4.3: Overlay of all constant distance plots

The experimental data collected is compared against the Penney & Hummert [10] data set and the equation given by Zheleznyak [6] in figure 4.4. The line corresponding to the Zheleznyak model [6] fits the data fairly well except at low values of pr. At about 50 cm-Torr, there is some deviation between both the line and data set. Perhaps a possible reason is different experimental conditions or experimental equipment. Another possible reason could be an incorrect calculated steradian value, which in this experiment is $1.5 \cdot 10^{-2}$. At pr > 50 cm-Torr, some of the data points are slightly higher in magnitude but for the most part converge with the Penney & Hummert data [10]. Since the data is close enough in shape and magnitude, this gives more confidence that the measured data is correct.

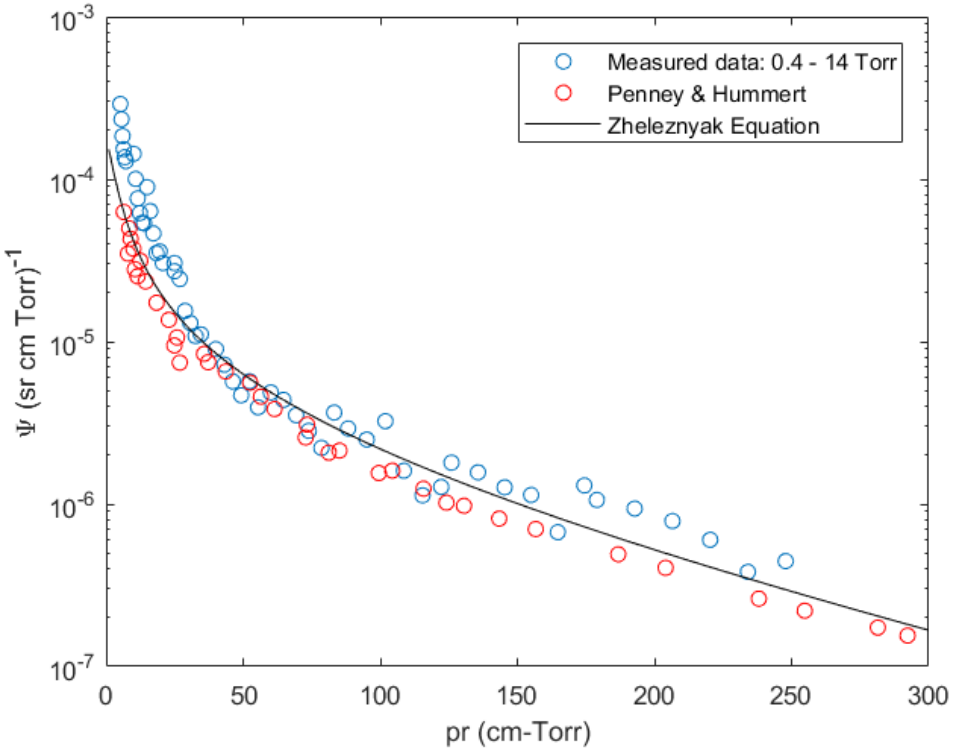

Figure 4.4: Comparing measured data vs Penney & Hummert [10] and Zheleznyak [6]

4.2 Effect of Varying Corona Current

Naidis [18] defines the amount of ionizing UV photons generated in the source chamber from the corona discharge as:

$$R_r = \int \omega v_d n_e dV \tag{4. 1}$$

where ω is the excitation coefficient of radiating states, v_d is the electron drift velocity and n_e is the electron density. Since the corona current is responsible for UV photon generation, equation 4.1 shows if the amount of excitations increases, then the amount of UV photons increases as well.

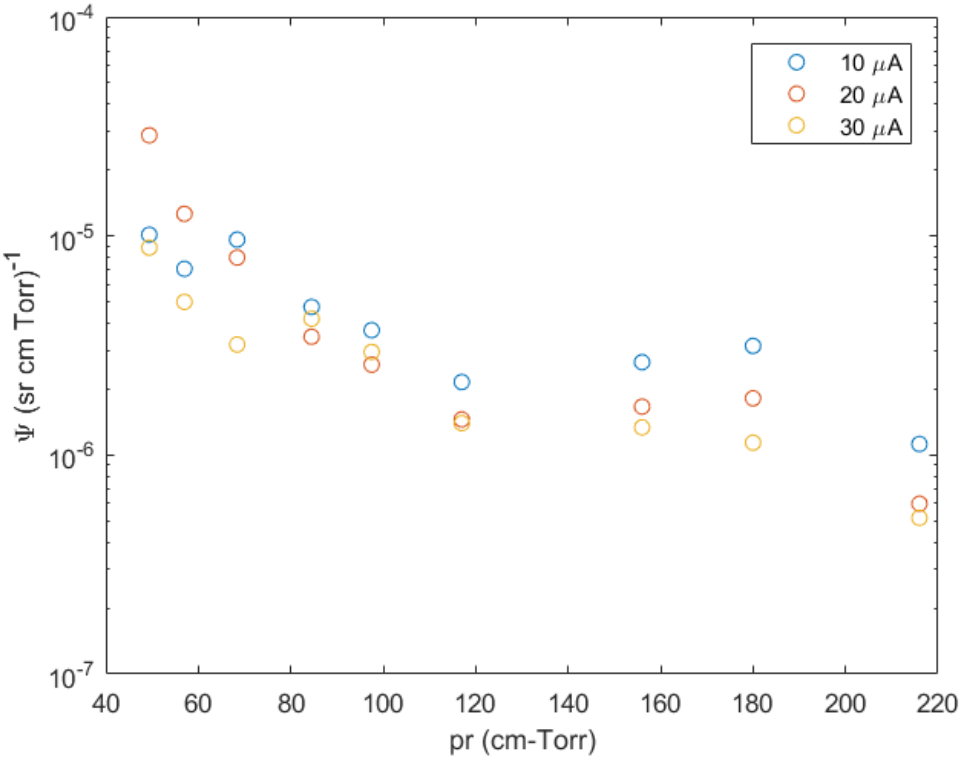

Figure 4.5: Effect of different source currents on Ψ

For various corona current values, figure 4.5 shows the effect of these corona current values on the photoionization coefficient. It is interesting to note when pr ≥ 80, the 10 μA corona current is expected to produce more photoionization in the collector chamber. Likewise, at low pr, the 20 μA corona current is expected to produce more photoionization than the 10 and 30 μA currents. Further investigation is needed to determine why different corona current values produces different amounts of photoionization since equation 4.1 shows that a higher excitation rate should produce more UV photons.

4.3 Effect of Varying Collector Voltage

All of the photoionization experiments [8 - 11] apply a voltage to the collector to measure the photoionization current. However, there is no data on varying the collector voltage to see the effect on photoionization. A higher applied voltage to the collector should

create a stronger electric field that can attract more ions and electrons produced from photoionization. The photoionization rate should have a strong dependence on the collector voltage. In figure 4.6, a test was performed that varied the collector voltage from 5 V to 20 V and measured the amount of photoionization.

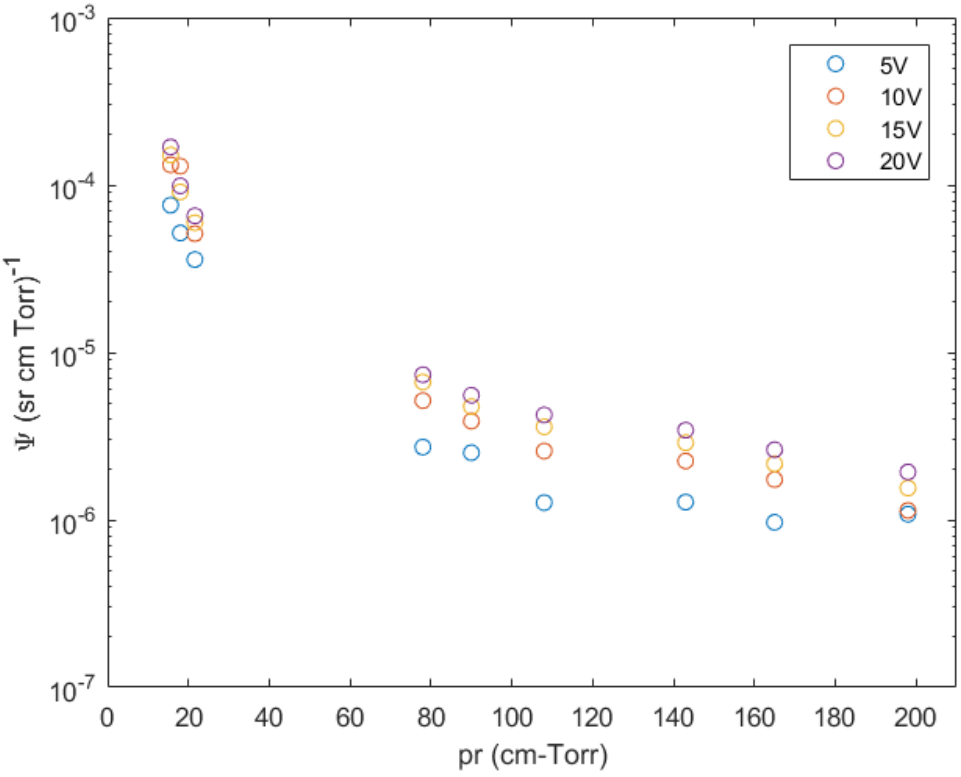

Figure 4.6: Effect of different collector voltages on Ψ

For each of the curves in figure 4.6, nine pressure values and three distance values were chosen to collect a few points to form a curve just to see the effect of voltage on the measured photoionization. Varying the collector voltage does seem to have an impact on the amount of photoionization measured. At low pr values, there is still a difference in varying the collector voltage but is not much as difference at higher pr. At higher pressures, there are a lot more molecules present in the chamber and applying a higher electric can separate the charges before any losses such as recombination can happen.

Chapter 5

Conclusion

An experimental setup capable of measuring the photoionization coefficient from a gas discharge was designed to compare the results of the widely used data set of Penney & Hummert [10] and the photoionization model given by Zheleznyak [6]. A discussion of results is presented along with future work.

5.1 Discussion

The measured photoionization coefficient in this experiment is in satisfactorily good agreement with the Penney & Hummert data set [10] and the model based on Zheleznyak [6]. However, there is some deviation between the measured data and Penney & Hummert data [10]. The greatest amount of deviation occurs when pr < 50 cm-Torr. One possible reason for this is in the experimental conditions between this experiment and theirs. In their setup, a constant pressure was maintained through the duration of each measurement. Whereas in this experiment, constant gas was injected into the chamber while simultaneously pumping the chamber. In a constant pressure chamber with no flow, there is some discharge byproducts that form in the source section [11]. These byproducts then change the absorption characteristics of the gas and affect the photoionization rate. As the N_2 emit UV photons, the byproducts in the source chamber absorb some of these photons does not make it into the collector chamber. With a constant flow of gas, any discharge byproducts are removed from the source chamber and more UV photons can travel to the collector chamber.

Penney & Hummert [10] mention in their paper that the ratio of collector current and corona current should have a slight curvature. When their data is plotted, they get straight lines with no curvature. Instead the ratio of their currents give a constant straight line. Figure 5.1 shows the ratio of collector current and corona current for pressures of 0.3 and 0.85 Torr that do show a slight curvature with them. This strengthens the validation that the measured photoionization coefficient is what should be measured.

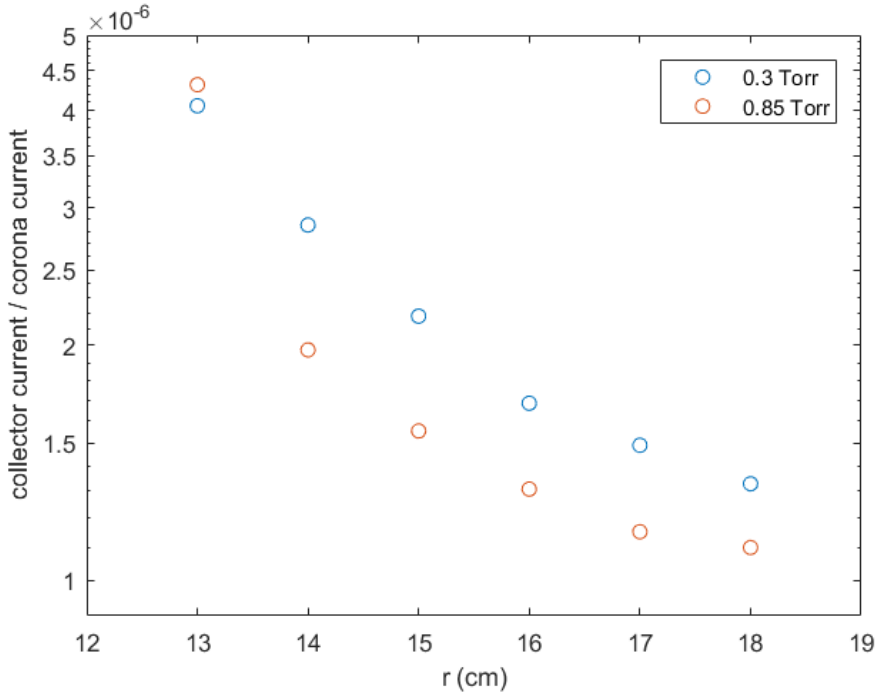

Figure 5.1: Ratio of collector current and corona current versus distance

5.2 Future Work

All of the photoionization measurements made were in dry air where the humidity is zero. The amount of humidity present in the system can change the characteristics of the gas. As the humidity increases, the amount of radiation absorbed by O_2 decreases since there is more molecules present. This reduces the amount of photoionization that occurs. It will be important to have photoionization data with humidity to incorporate in simulations.

Changing the mixtures of $N_2 - O_2$ can yield some useful information since photoionization occurs upon absorption of O_2. By changing, the concentration of O_2 of a given mixture can change the rate of photoionization and therefore changes the streamer behavior when performing simulations.

In the experimental setup, an aperture separates the source chamber from the collector chamber. The corona discharge contains a wide spectrum of photons emitted that can pass into the collector chamber. These photons may not be in the bands listed by [6]. If a filter is placed in front of the aperture that allows a band of radiation to pass through, then it will be easier to identify which of these bands is the most dominant at photoionizing O_2. Furthermore, this can potentially help identify other bands that may not have been considered that can photoionize O_2.

Perhaps the most important work moving forward is determining what the quenching pressure of air is in air and in other gases. Quenching refers to the process of a non-radiative transition from an excited state to a lower state via collisions as shown in figure 5.2.

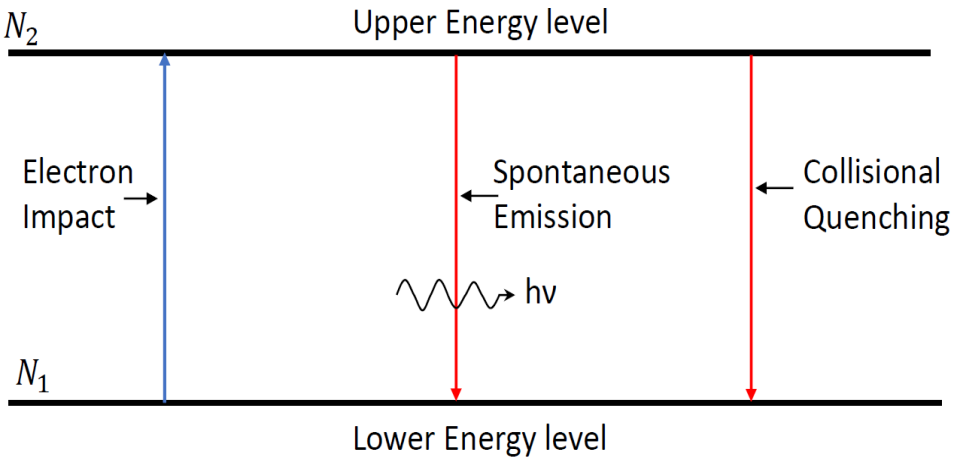

Figure 5.2: Two level energy diagram

In the case of air, as the N_2 molecules are excited to higher electronic states, they collide with another molecule. This collision causes the electrons to return to the ground state

without emitting a photon. The energy that would have resulted in a photon is converted to a different form of energy. As the pressure increases, many more collisions start to occur and eventually the frequencies of these collisions starts becoming higher than the emission rate. This causes the photoionization rate to decrease as the pressure increases. Currently, there is only one proposed value for the quenching pressure first proposed by Teich [9] as a value of 30 Torr. This quenching pressure value is often used to scale the overall photon output in the photoionization source term [e.g. 4]. This quenching pressure does not explain the physics involved in the quenching processes. Moving forward, this experimental setup will be used to help in determining the quenching pressure and the processes of quenching for use in computational codes.

References

[1] N. Liu, V. P. Pasko, "Effects of photoionization on propagation and branching of positive and negative streamers in sprites", *Journal of Geophysical Research*, vol. 109, no. A4, A04301, 2004

[2] J. Stephens, A. Fierro, S. Beeson, G. Laity, D. Trienekens, R. P. Joshi, J. Dickens and A. Neuber, "Photoionization capable, extreme and vacuum ultraviolet emission in developing low temperature plasmas in air", *Plasma Sources Science and Technology*, vol. 25, no. 2, pp. 1-11, 2016

[3] W. J. Yi and P. F. Williams, "Experimental study of streamers in pure $N_2$and N_2/O_2 and a ≈13 cm gap", *Journal of Physics D: Applied Physics*, vol. 35, no. 3, pp. 205-218, 2002

[4] M. M. Nudnova, A. Yu. Starikovskii, "Streamer head structure: role of ionization and photoionization", *Journal of Physics D: Applied Physics*, vol. 41, no. 23, pp. 1-11, 2008

[5] S. Nijdam, F. M. J. H. van de Wetering, R. Blanc, E. M. van Veldhuizen and U. Ebert, "Probing photo-ionizing: experiments on positive streamers in pure gases and mixtures ", *Journal of Physics D: Applied* Physics, vol. 43, no 14, pp. 1-16, 2010

[6] M. B. Zheleznyak, A. K Mnatsakanyan, S. V. Sizykh, "Photoionization of Nitrogen and Oxygen mixtures by radiation from a gas discharge", *High Temp.*, vol. 20, no. 3, pp. 357-362

[7] S. Pancheshnyi, "Photoionization produced by low-current discharges in O_2, air, $N_2$and CO_2", *Plasma Sources Science and Technology*, vol. 24, no. 1, pp. 1-19, 2015

[8] A. Przybylski, “Untersuchung über die „gasionisierende“ Strahlung einer Entladung“, *Zeitschrift für Physik,* vol. 151, no. 3, pp. 264-280, 1958

[9] T. H. Teich, “Emission gasionisierender Strahlung aus Elektronenlawinen I. Meßanordnung und Meßverfahren. Messungen in Sauerstoff“, *Zeitschrift für Physik,* vol. 199, no. 4, pp. 378-394, 1967

[10] G. W. Penney and G. T. Hummert, “Photoionization Measurements in Air, Oxygen, and Nitrogen”, *Journal of Applied Physics,* vol. 41, no. 2, pp. 572-577, 1970

[11] M. Aints, A. Haljaste, T. Plank and L. Roots, “Absorption of Photo-Ionizing Radiation of Corona Discharges in Air”, *Plasma Processes and Polymers*, vol. 5, no.7, pp. 672-680, 2008

[12] A. A. Kulikovsky, “The role of photoionization in positive streamer dynamics”, *Journal of Physics D: Applied. Physics*, vol. 33, no. 12, pp. 1514-1524, 2000

[13] S. Pancheshnyi, “Role of electronegative gas admixtures in streamer start, propagation and branching phenomena”, *Plasma Sources Science and Technology*, vol. 14, no. 4, pp. 645-653, 2005

[14] A. Luque, U. Ebert, C. Montijn and W. Hundsdorfer, “Photoionization in negative streamers: Fast Computations and two propagation modes”, *Applied Physics Letters,* vol. 90, no. 8, 1-3, 2007

[15] A. Bourdon, V. P. Pasko, N. Y. Liu, S. Célestin, P. Ségur and E. Marode, “Efficient models for photoionization produced by non-thermal gas discharges in air based on

radiative transfer and the Helmholtz equations", *Plasma Sources Science and Technology*, vol. 16, no. 3, pp. 656-678, 2007

[16] G. Wormeester, S. Pancheshnyi, A. Luque, S. Nijdam, and U. Ebert, "Probing photo-ionization: simulations of positive streamers in varying N_2: O_2-mixtures", *Journal of Physics D: Applied Physics*, vol. 43, no. 50, pp. 1-13, 2010

[17] B. Bagheri and J. Teunissen, "The effect of the stochasticity of photoionization on 3D streamer simulations", *Plasma Sources Science and Technology*, vol. 28, no. 4, pp. 1-10, 2019

[18] G. V. Naidis, "On photoionization produced by discharges in air", *Plasma Sources Science and Technology*, vol. 15, no. 2, pp. 253-255, 2006

[19] J. Lehr and P. Ron, Foundations of Pulsed Power Technology, New Jersey: John Wiley & Sons, 2017

[20] J. M. Meek and J. D. Craggs, Electrical Breakdown of Gases, Oxford Press, 1953

[21] J. M. Meek and J. D. Craggs, Electrical breakdown of gases, Wiley, 1978

[22] G. V. Marr, Plasma Spectroscopy, Elsevier Publishing Company, 1968

[23] A. P. Thorne, Spectrophysics, Chapman and Hall, 1974

[24] Herzberg, Spectra of Diatomic Molecules, 1950

[25] C. W. Walter, P. C. Cosby and H. Helm, " Photoexcitation and predissociation intensities of the $c'^1\Sigma_u^+$ (v=3 and 4), $c^1\Pi_u$ (v=3 and 4), and $b'^1\Sigma_u^+$ (v=10, 12, 13 and 15) states of N_2", *Journal of Chemical Physics*, vol. 112, no. 10, pp. 4621-4633, 2000

[26] Keithley Instruments, “2410 Model Datasheet”, [Online], Available: https://www.tek.com/datasheet/series-2400-sourcemeter-Instruments

[27] Keithley Instruments, “6430 Model Datasheet”, [Online], Available: https://www.tek.com/datasheet/high-resistance-low-current-electrometers-series-6500-6430/model-6430-sub-femtoamp-remote-

[28] Keithley Instruments, ‘Low Level Measurements Handbook: Precision DC Current, Voltage, and Resistance Measurements”, 7th Edition,